



# Modification of Diss Fibers for Biocomposites Based on Recycled Low-Density Polyethylene and Polypropylene Blends

Zohra Touati<sup>1,2</sup> · Hakima Boulahia<sup>2</sup> · Naima Belhaneche-Bensemra<sup>1</sup>  · Valérie Massardier<sup>3</sup>

Received: 26 September 2017 / Accepted: 5 February 2018 / Published online: 13 February 2018  
© Springer Science+Business Media B.V., part of Springer Nature 2018

## Abstract

The aim of this work is the valorization of diss fibers with recycled and regenerated low-density polyethylene (rLDPE) for the development of biocomposites based on blends of rLDPE polypropylene (PP) and diss fibers. The diss fibers were characterized by laser granulometer and FTIR spectroscopy. Two PP/rLDPE blends of different compositions (50/50 and 75/25) were prepared. These polymer blends were reinforced by nano-Si particles and compatibilizers which were investigated using three compatibilizers: maleic anhydride functionalized ethylene copolymer rubber (MAC), maleic anhydride functionalized ethylene copolymer rubber/SiO<sub>2</sub> (MAC/SiO<sub>2</sub>), and maleic anhydride functionalized ethylene copolymer rubber/SiO<sub>2</sub>/ionic liquid (MAC/SiO<sub>2</sub>/IL). The thermal properties of the blends were studied using differential scanning calorimetry and thermogravimetric analysis. Their crystallinity was investigated by X-ray diffraction and their morphology by scanning electron microscopy, while mechanical properties were evaluated by tensile testing. The best tensile properties were obtained for the PP/rLDPE (75/25) blend. A significant increase of the Young's modulus, stress at break, and elongation at break was obtained with the three compatibilizers. MAC acted as a compatibilizer of both polymers, resulting in improved interfacial adhesion which increased tensile properties. Finally, the effect of diss fiber surface modification on the properties of PP/rLDPE blends was considered. The results showed a modification of tensile properties and a satisfactory interfacial adhesion between diss fibers and polymer blends. Furthermore, thermal stability was not significantly decreased by the addition of 5 wt% diss fibers.

**Keywords** Recycled and regenerated low-density polyethylene · Polypropylene · Blends · Compatibilizer · Diss fibers · Composites · Tensile properties · Thermal properties

## Introduction

Every year, a few million tons of wastes from plastic manufacturers are collected all over the world. Over time, the capacity of recycling plastic wastes gradually increased. However, the percentage of plastics found in landfills is still very significant [1]. Some of the most important commodity polymers include polypropylene (PP), high-density polyethylene (HDPE), and low-density polyethylene (LDPE)

[2–5]. All of these polymers are derived from petrochemical resources and have long chains of hydrogen and carbon atoms. While polyethylene (PE) is in the first place with 32%, polypropylene (PP) is in the second place with 20% followed by poly (vinyl chloride) (PVC) with 17% in manufacturing and consumption of plastics in the world this indeed causes a large amount of post-consumer waste of this polymer. Polyolefins, especially polyethylene (PE) and polypropylene (PP), have been widely used due to their relative low density, good chemical resistance, electrical insulation properties, and low cost. It is therefore desirable to prepare superior polyolefin blends for use in applications such as packaging, pipe, wire and cable, and other insulation materials [6].

More recently, issues related to sustainable development and environmental preservation are receiving significant attention from the global community. The advantages of recycled polymers include reduction of energy consumption compared to virgin polymers, lowering the disposal of

✉ Naima Belhaneche-Bensemra  
naima.belhaneche@g.enp.edu.dz

<sup>1</sup> Laboratoire des Sciences et Techniques de l'Environnement, Ecole Nationale Polytechnique, BP 182, El-Harrach, Algiers, Algeria

<sup>2</sup> Materials, Processes and Environment Research Unit, M'Hamed Bougara University, Boumerdes, Algeria

<sup>3</sup> Engineering of Polymer Materials, University of Lyon, CNRS, UMR, INSA, Lyon, France

plastic wastes in garbage cans, and creating jobs and income. The recycling of industrial scraps is a successful practice because of the low level of contamination. Recycling municipal plastic wastes is often a delicate task, as these materials are usually a mixture of different polymers, making treatment more difficult and also limiting the number of potential applications [7].

The traditional solutions of handling the waste plastics are landfill, incineration, and recycling [8], but the former two are undesirable because that would either cause pollutions or emit harmful gases. Taking waste PVC as an example, when burnt, it can emit toxic gases such as dioxins [9]. Obviously, recycling is an appropriate way because of its efficiency and reuse. There are four main methods of plastic waste recycling [10]: energy recovery, feedstock recycling, chemical recycling, and material recycling. Adding plastic recyclates to the original material is an important issue in terms of managing growing amounts of various polymer waste materials [11–13]. Recently, a great attention is being paid on the use of different polymer-based materials including recycled polymers as matrices for reinforcement with nanomaterials to develop innovative nanocomposite materials [14–18].

Diss (*Ampelodesma mauritanica*) is a large grass widespread growing in the Mediterranean North Africa and in the dry regions of Greece to Spain. In France, it is found in the departments of Var, Southern Corsica, and Hérault. This plant was previously used in the realization of the old dwellings because of its mechanical and physical properties [19]. Its fibrous nature may be capable of offering interesting properties to composite materials.

The aim of this work is the valorization of diss fibers with recycled and regenerated low-density polyethylene (rLDPE) for the development of biocomposites based on blends of rLDPE/polypropylene and diss fibers. Blends of PP and rLDPE may contribute to make recycling more economically attractive.

In mixtures rich in LDPE, a heterogeneous distribution of PP in the LDPE matrix corresponds to a biphasic system in the molten state [20–22]. The lack of interfacial adhesion between both phases results in a decrease in the mechanical properties, in particular regarding morphology, impact resistance, breaking stress, and ductile to brittle transition. According to Radonjic and Gubeljic [23], the immiscibility between both phases makes the rule of mixtures ineffective in the prediction of some properties of interest. To overcome this difficulty, the use of various coupling agents was reported. It was found that the addition of ethylene/propylene block copolymer enhances the ductility of LDPE/PP mixtures, especially mixtures with high PP percentages [23–25]. Hanks et al. [21] used ethylene-propylene-diene copolymer (EPDM) or PE-g (2-methyl-1,3-butadiene) to improve stress and elongation at break of virgin and recycled

LDPE/PP. Inorganic particulate fillers such as micro-/nano-SiO<sub>2</sub> nanoparticles [26, 27], nCaCO<sub>3</sub>, carbon nanotubes and laminated silicates [4, 27–30] were used to make polymer composites. They were reported to combine the advantages of their constituent phases. Nano-SiO<sub>2</sub> which exhibit interesting physicochemical properties has the great advantage of reinforcing the polymers. Silica nanocomposites exhibit improved thermal stability, enhanced mechanical properties, decreased gas permeability, and reduced flammability compared to pure polymers [31–35]. In PP and LDPE mixtures, maleic anhydride functionalized ethylene rubber copolymer was shown to limit the problem of aggregation of the silica within the matrix as it consists of two parts; the hydrophobic part is miscible with the polypropylene matrix while the hydrophilic part can interact with the hydroxyl groups present on the entire surface of the nano-SiO<sub>2</sub>. Blends and compatibilized blends can be prepared by various methods such as solution mixing [36], in situ spacer polymerization [37], and sol-gel reaction [38–40]. Recently, ionic liquids (ILs), especially known for their excellent thermal and chemical stability, their non-flammability, and their low saturated vapor pressure, were used as surfactants, lubricants, plasticizers, building blocks, or processing aids of polymer matrices [41–49]. Leroy et al. [50] studied the starch-zein melt processed blends following the utilization of an ionic liquid as plasticizer agent.

Increased pressure from society, preservation of natural resources as well as rigor of laws adopted by developing countries lead to the invention and development of natural materials based on renewable raw materials [51]. In this context, composites need to use natural plant-based fibers such as linen, diss, jute, sisal, kenaf, banana as alternative materials to replace solid wood. Reinforced polymer composites based on cellulosic fibers have been used for many applications such as automotive components, aerospace parts, sporting goods as well as construction materials. Reinforced polymer composites based on cellulosic fibers have found major applications in the construction of bridges and buildings in recent years. This is due to the advantageous properties of these materials, such as low weight, high strength, free formability, and substantial resistance to corrosion and fatigue. The disadvantage is the lack of compatibility between the polymer matrix and the natural fibers, which reduces the final performances of material, thus limiting the possible applications [3, 4]. This is due to the hydrophilic character of the natural fibers with respect to the polymer matrix which has a hydrophobic character. To improve the adhesion between the polymer matrix fibers, various chemical and physical methods have been elaborated [2, 5].

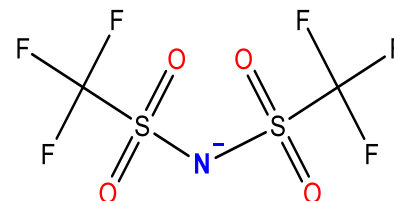
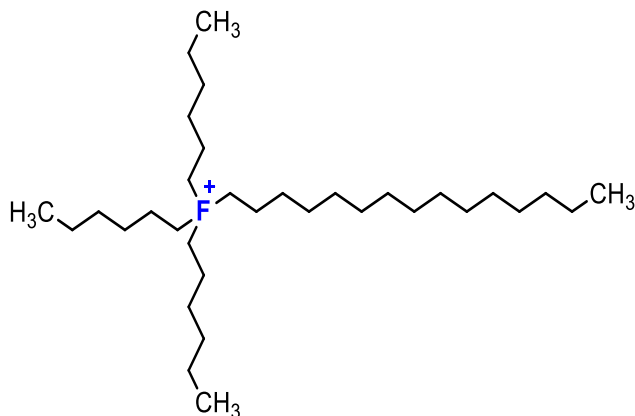
In the present work, PP/rLDPE blends of variable compositions (75/25 and 50/50) were prepared and reinforced by maleic anhydride functionalized ethylene copolymer rubber/SiO<sub>2</sub> and maleic anhydride functionalized ethylene

copolymer rubber/SiO<sub>2</sub>/ionic liquid. Their morphological, thermal, and mechanical properties were evaluated. The chemical composition of the diss grass is mainly lignin, cellulose, and hemicellulose. The insufficient interface quality between the diss and the polymer matrix is the first and the most important problem in natural fiber-reinforced composites. Diss fibers were thermally and chemically treated to be used as reinforcements of compatibilized PP/rLDPE blends. The mechanical, thermal properties, and morphologies of the composites were investigated.

## Experimental

### Materials

Isotactic polypropylene was supplied by Sabic V R (Saudi Arabia). The sample properties were as follows: flow index (MFI) of 10 g/10 min (2.15 kg at 230 °C), melting point of 164.4 °C, and a crystallinity percentage of 38.6%. Regenerated low-density polyethylene was supplied by “UTPS Imprimeurs sur matières plastiques” (Algeria). It was obtained from recycled trash bins with non-contaminated waste. Samples had a density of 0.918 g/cm<sup>3</sup> and a melt flow index of 7.5 g/10 min. Maleic anhydride functionalized ethylene copolymer rubber (Exxelor VA 1801) was provided by Exxon Mobil (France). Hydrophilic fumed silica nano-SiO<sub>2</sub> was supplied by Degussa GmbH (Germany) under the trade name AEROSIL OX 50. Average primary particle size was of 40 nm, the specific surface area of 50 m<sup>2</sup>/g, and the nano-SiO<sub>2</sub> content of 99.8%. The ionic liquid-based phosphonium cations with different anions (trihexyl tetradecyl phosphonium bis (trifluoro methyl sulfonyl) imide, termed IL-TFSI) having a molar mass *M* of 764 g mol<sup>-1</sup> and supplied by Cytec industries Inc (Scheme 1). The commercial name is Cyphos-IL109. Diss fibers were collected in the Algerian province of Msila between March and June 2016.



**Scheme 1** Chemical structures of the IL-TFSI ionic liquid

## Surface Modification of Diss Fibers

### Thermal Treatment

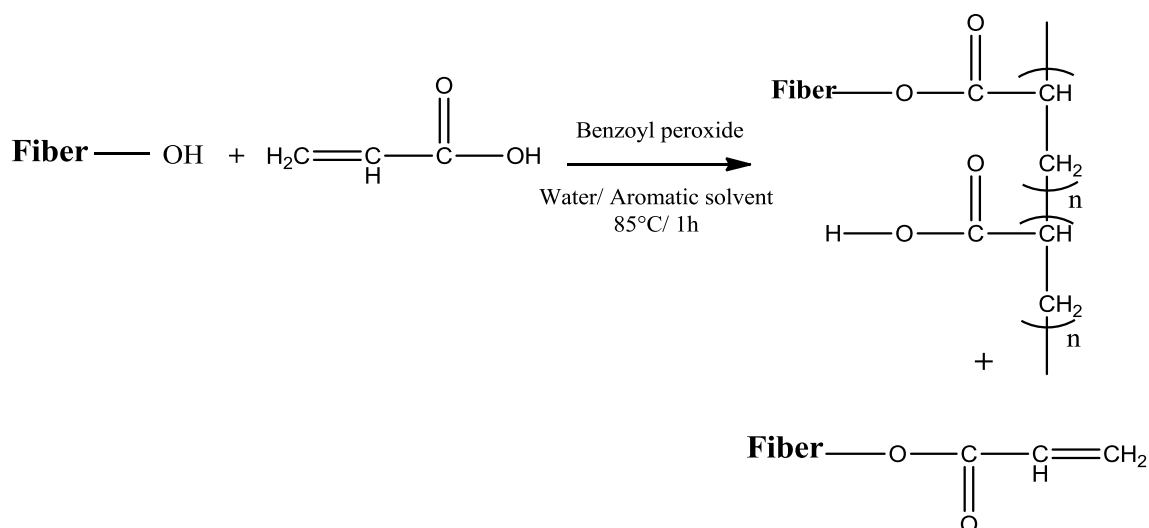
Diss fibers were washed with water to remove contaminants and dust. They were dried at room temperature and cut into 1 cm length. Diss fibers were chopped with a blade crusher. The particle size was analyzed by laser granulometry. Chopped diss fibers were subjected to heat treatment by keeping samples in an oven at 100 °C during 4 h.

### Chemical Treatment

Chemical treatment was performed according to the method described by Bessadok et al. [52] with several adaptations. Diss fibers were firstly swelled in a water/aromatic solvent (45/5 cm<sup>3</sup>) for 15 min at 85 °C. Then, fibers were modified with acrylic acid monomer (AA) (0.3 M) using benzoyl peroxide (POB) (0.01 M) as an initiator for 1 h at 85 °C (Scheme 2). The modified fibers were firstly washed with an alkaline solution (1 g L<sup>-1</sup> NaOH and 6 g L<sup>-1</sup> NaCl) for 15 min, then with distilled water for 1 h. Finally, the modified fibers were dried in an oven at 60 °C for 12 h and cooled in a desiccator.

### Preparation of Polymer Blends and Biocomposites

The PP/rLDPE (50/50 and 75/25 by weight) blends and compatibilized PP/rLDPE blends [PP/rLDPE/MAC (47.5/47.5/5); PP/rLDPE/MAC/SiO<sub>2</sub> (46/46/5/3); PP/rLDPE/MAC/SiO<sub>2</sub>/IL (44.5/44.5/5/3/3); PP/rLDPE/MAC (63.3/31.7/5); PP/rLDPE/MAC/SiO<sub>2</sub> (61.3/30.7/5/3); PP/rLDPE/MAC/SiO<sub>2</sub>/IL (59.3/29.7/5/3/3)] were prepared by using a twin-screw co-rotating extruder (Coperion ZSK18K38, screw diameter of 18 mm, L/D = 44), operating at 100 rpm with a constant feed ratio of 2.5 kg/h. The temperature profile was 180, 190, and 200 °C. The tensile



**Scheme 2** Impact of acrylic acid treatment on cellulosic fibers

samples were then prepared by injection molding with a Battenfeld injection molding machine, keeping the temperature of the barrel at 200 °C, and the mold at 25 °C. Based on the formulation PP/rLDPE/MAC/SiO<sub>2</sub> (63.3/31.7/5/3) and the same operating conditions, biocomposites were prepared by adding either 5 wt% of untreated diss fibers (UDF) [PP/rLDPE/MAC/SiO<sub>2</sub>/UDF (58/29/5/3/5)], or 5 wt% thermally treated diss fibers (TTDF) [PP/rLDPE/MAC/SiO<sub>2</sub>/TTDF (58/29/5/3/5)] or 5 wt% chemically treated diss fibers PP/rLDPE/MAC/SiO<sub>2</sub>/CTDF (58/29/5/3/5).

## Characterization Methods

### Particle Size Analysis

Diss particle size analysis was performed by a laser granulometer (Malvern Instruments Ltd, Worcestershire, UK).

### Fourier Transform Infrared Spectroscopy

The efficiency of thermal and chemical treatments of the fibers was studied by FTIR analysis in attenuated total reflectance mode (ATR), using a Nicolet Avatar 360 FTIR spectrophotometer. Two hundred scans were collected for each measurement over the spectral range 4000–400 cm<sup>-1</sup> with a resolution of 4 cm<sup>-1</sup>. The IR spectra were presented in absorbance and assembled on a common scale.

### Tensile Testing

The tensile tests were conducted using an Instron testing machine with a crosshead rate maintained at 5 mm/min.

The test was conducted following the ASTM D638 standard. Five measurements were conducted and an average for the final result was considered. The dimensions of the calibrated part involved a width of 4 mm, a thickness of 3 mm, and a length of 40 mm.

### Differential Scanning Calorimetry

The study of the crystallization behavior of the samples was carried out using a differential scanning spectrophotometer (DSC model Q10) under nitrogen atmosphere. Indium and tin were used for the calibration of both heat of fusion and melting temperature. The samples were first heated up from 25 to 200 °C (first heating cycle). Then, they were cooled down from 200 to -60 °C (cooling cycle) and finally they were heated up again from -60 to 200 °C (second heating cycle). The value -60 °C corresponds to the limit of the device. The heating and cooling rates were maintained at 10 °C/min in all the different cycles. The enthalpies of fusion and crystallization of the rLDPE and PP phases were calculated from the DSC curves by integrating the appropriate peaks. Then the degree of crystallinity ( $X_c$  %) of the different biocomposites was calculated from the values of enthalpy of fusion of the different phases ( $\Delta H_{m,rLDPE}$  and  $\Delta H_{m,PP}$ ) and the heat of fusion of perfectly crystalline polyethylene (289, 9 J/g [53]) and polypropylene (209 J/g [54])) as shown in Eqs. (1) and (2).

$$X_{\%rLDPE} = \frac{\Delta H_{m,rLDPE}}{w\Delta H_{m,LDPE}^0} 100 \quad (1)$$

$$X_{\%PP} = \frac{\Delta H_{m,PP}}{w\Delta H_{m,PP}^0} 100 \quad (2)$$

## Thermogravimetric Analysis

Thermal gravimetric (TG) and derivative thermal gravimetric (DTG) analyses were carried out using a TGA Q500 TA instrument in an inert atmosphere at a heating rate of 10 °C/min. The samples weights were in the [10–20 mg] range and were scanned from 25 to 600 °C.

## X-ray Diffraction Analysis

The crystalline structures of PP/rLDPE compatibilized and reinforced by MAC, MAC/SiO<sub>2</sub>, and MAC/SiO<sub>2</sub>/IL were evaluated by X-ray diffraction (XRD) analysis. XRD measurements were carried out by an Advance D8X-ray diffractometer operating with a Cu K $\alpha$  radiation source. The X-rays were generated at 40 kV and 27 mA power and XRD scans were recorded at 2 $\theta$  from 1° to 50°.

The percentage of crystallinity can be determined from Eq. (3).

$$\% \text{ Crystallinity} = \frac{\text{Area under crystalline peak}}{\text{Total area under all peaks}} \times 100 \quad (3)$$

## Scanning Electron Microscopy Analysis

The morphologies of compatibilized PP/rLDPE blends by MAC, MAC/SiO<sub>2</sub>, and MAC/SiO<sub>2</sub>/ionic liquid were observed by scanning electron microscopy (SEM) technique. SEM observations were performed using a Quanta 250 (model) FEI (manufacturer) with a 5 kV voltage. The samples were fractured in nitrogen and then metalized with a mixture of Au/Pd.

## Results and Discussion

### Diss Fibers Characterization

#### Particle Size Analysis

This particle size analysis consists in determining the size or the diameter of the particles by a laser beam. The spectrum gives the quantity (volume) as a function of the particles size. The average diameter of the untreated diss fibers is of the order of 570  $\mu\text{m}$  as shown by the particle size analysis (Fig. 1).

#### FTIR Spectroscopy Analysis

The efficiency of the thermal and chemical treatments on the fibers was studied by ATR spectroscopy by comparing the IR spectra of the fibers before and after each treatment

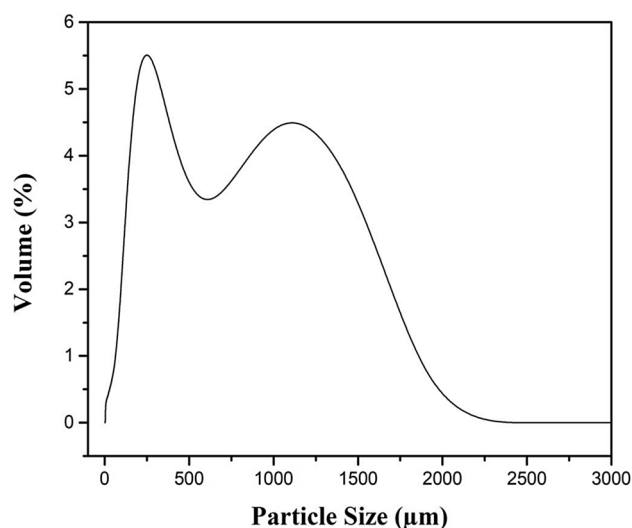


Fig. 1 Laser granulometric analysis of untreated diss fibers

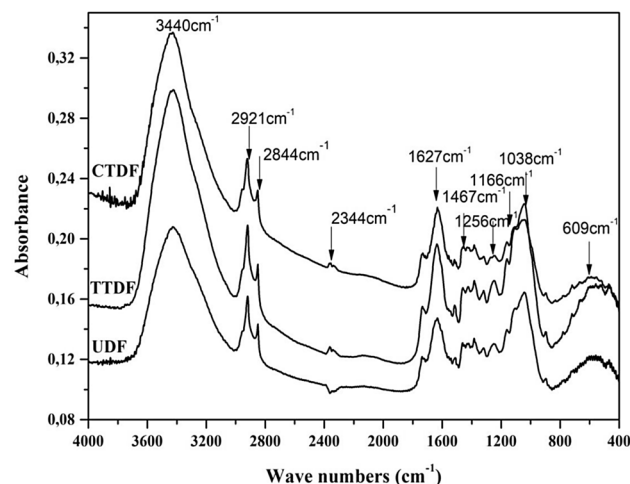


Fig. 2 FTIR-ATR spectra of the untreated (UDF), thermally (TTDF), and chemically treated diss fibers (CTDF)

(Fig. 2). The main absorbance peak reflecting the C–C cycle of the carbohydrate skeleton of cellulose appears at 1160  $\text{cm}^{-1}$  [55–57]. Diss is mainly composed of cellulose, hemicellulose, lignin, and of some pectin's. On the untreated fiber spectra, the C–O–C cellulose glycosidic bond was detected by the stretching vibration band at 1100  $\text{cm}^{-1}$ . The C–OH of the cellulosic backbone, secondary C–O alcohols and C–O primers were observed at 1056 and 1030  $\text{cm}^{-1}$ , respectively. Peaks due to alcoholic cellulose groups (OH deformation) were located at 1360 and 1320  $\text{cm}^{-1}$  while the band at 1315  $\text{cm}^{-1}$  corresponds to  $-\text{CH}_2-$  wagging of cellulose. The 1426  $\text{cm}^{-1}$  band was attributed to cellulose  $-\text{CH}_2-$  bending. The large low absorbance peak at 1650  $\text{cm}^{-1}$  is due to the presence of

lignin [37, 38]. The band observed in the  $3340\text{ cm}^{-1}$  region is mainly bound to OH groups. The spectra of CTDF and TTDF were compared to the spectrum of untreated fibers (Fig. 2). The band observed at  $3340\text{ cm}^{-1}$  was reduced for both TTDF and CTDF. The heat treatment does not greatly affect the surface of the fibers (Fig. 2). Only an increase in crystallinity and moisture removal occurs for dissolution after heat treatment. The increase in crystallinity of the fiber was also observed by Sreekumar et al. [60]. For CTDF treatment, this observation can be explained by the addition of  $\text{CH}_2$  and  $-\text{CH}-$  groups on the fibers [57]. The advantage of adding  $\text{CH}_2$  and  $\text{CH}$  groups is the reduction of the hydrophilic nature of the diss fiber and thus the improvement of the interfacial adhesion between the fiber and the matrix.

When comparing the spectra of CTDF and TTDF to that of untreated fibers, the band observed at  $3340\text{ cm}^{-1}$  was reduced for both treated fibers. This was due to the diminution of hydroxyl groups derived from these treatments.

The new peaks located at  $2900\text{--}2850\text{ cm}^{-1}$  were more marked in the AA spectra compared to untreated spectrum because these treatments lead to  $-\text{CH}_2-$  and  $-\text{CH}-$  group formation onto the fiber and the conjugation with carbonyl group had a marked effect and the group ( $\text{C}=\text{CH}-\text{COOR}$ ) absorbed near  $810\text{ cm}^{-1}$  [58–60].

### XRD Characterization

The X-ray diffraction pattern of UDF, CTDF, and TTDF is illustrated in Fig. 3 by a Bragg angle function ( $2\theta$ ). For cellulose, three main peaks were observed at  $2\theta = 15.3^\circ$ ,  $2\theta = 22.4^\circ$ , and  $2\theta = 34.6^\circ$  corresponding to the diffraction of the plane (110) of the amorphous cellulose while  $2\theta = 22.4^\circ$  and  $2\theta = 34.6^\circ$  correspond, respectively, to the diffractions of the

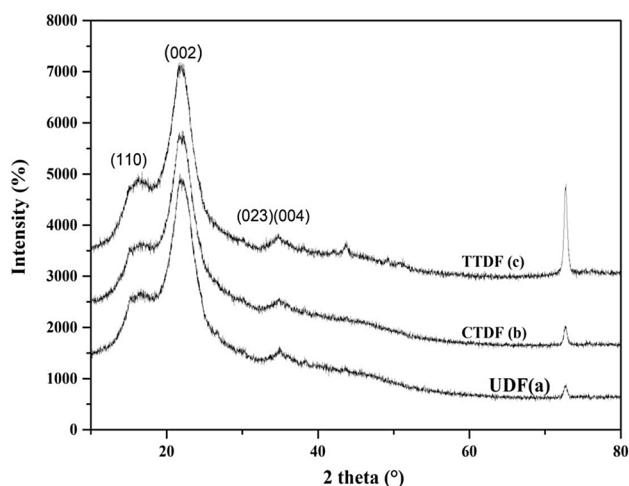


**Fig. 3** X-ray diffraction of untreated (UDF), thermally (TTDF), and chemically treated diss fibers (CTDF)

planes (002) and (004) and are attributed to the crystalline form of the cellulose as observed by Uma Maheswari et al. and by Haibo Zhao et al. for the X-ray analysis of extracted cellulose microfibrils [46].

The heat treatment does not greatly affect the surface of the fibers. Only an increase in crystallinity and moisture removal occurs for dissolution after heat treatment. The increase in crystallinity of the fiber was also observed by Sreekumar et al. [60].

From the different X-ray curves, the crystallinity values of the fibers after each treatment were calculated and presented in Table 1. In regard to these results, the thermal treatment was proved to achieve a huge increase of crystallinity. The growth of the fiber crystallinity owing to heat treatment has already been pointed out by Sreekumar et al. [60]. Concerning the chemical treatments, almost all achieved an increase in the fiber crystallinity. The highest value was seen for the acrylic acid treated-fiber (CTDF) whose crystallinity was similar to that of the thermal treatment owing to the grafting of groups  $\text{CH}$  and  $\text{CH}_2$ .

### Compatibilized PP/rLDPE Blends and Biocomposites Characterization

#### Tensile Testing

The Young's modulus, stress, and elongation at break of uncompatibilized blends (PP/rLDPE: 50/50 and 75/25), compatibilized blends [PP/rLDPE/MAC (47.5/47.5/5); PP/rLDPE/MAC/SiO<sub>2</sub> (46/46/5/3); PP/rLDPE/MAC/SiO<sub>2</sub>/IL (44.5/44.5/5/3/3); PP/rLDPE/MAC (63.3/31.7/5); PP/rLDPE/MAC/SiO<sub>2</sub> (61.3/30.7/5/3); PP/rLDPE/MAC/SiO<sub>2</sub>/IL (59.3/29.7/5/3/3)] and biocomposites [PP/rLDPE/MAC/SiO<sub>2</sub>/untreated and treated diss fibers (58/29/5/3/5)] are illustrated in Table 2. Tensile properties decreased when lowering the level of rLDPE in the blends [Young's modulus from 560.2 MPa for PP/rLDPE (50/50) to 581.9 MPa for PP/rLDPE (75/25)], stress at break [from 30.5 MPa for PP/rLDPE (50/50) to 35.9 MPa for PP/rLDPE (75/25)], and elongation at break [from 759.1% for PP/rLDPE (50/50) to 824.9% for PP/rLDPE (75/25)]. These poor mechanical performances are related to the immiscibility of the polymers. In order to enhance the compatibility of our pair of polymers, three compatibilizers and reinforcement systems

**Table 1** Crystallinity ( $X_c$  %) of the untreated (UDF), thermally (TTDF), and chemically treated diss fibers (CTDF)

Formulations	Crystallinity ( $X_c$ %)
UDF	40.3
CTDF	79.6
TTDF	83.3

**Table 2** Tensile properties of uncompatibilized, compatibilized PP/rLDPE blends, and biocomposites: Young modulus, tensile strength, and elongation at break

Formulations	Young's modulus (MPa)	Tensile strength (MPa)	Elongation at break (%)
PP/rLDPE (50/50)	560.2 ± 4.9	30.5 ± 0.5	759.1 ± 1.9
PP/rLDPE/MAC (47.5/47.5/5)	559.8 ± 1.7	33.5 ± 0.4	805.3 ± 6.4
PP/rLDPE/MAC/SiO <sub>2</sub> (46/46/5/3)	597.3 ± 5.6	35.1 ± 0.4	880.4 ± 5.5
PP/rLDPE/MAC/SiO <sub>2</sub> /IL (44.5/44.5/5/3/3)	572.2 ± 2.4	31.1 ± 0.4	799.5 ± 1.6
PP/rLDPE (75/25)	581.9 ± 2.7	35.9 ± 0.6	824.9 ± 6.2
PP/rLDPE/MAC (63.3/31.7/5)	561.0 ± 2.5	33.5 ± 1.3	937.0 ± 0.0
PP/rLDPE/MAC/SiO <sub>2</sub> (61.3/30.7/5/3)	655.4 ± 5.9	34.1 ± 0.4	883.6 ± 5.3
PP/rLDPE/MAC/SiO <sub>2</sub> /IL (59.3/29.6/5/3/3)	622.1 ± 1.4	31.8 ± 0.4	844.2 ± 4.7
PP/rLDPE/MAC/SiO <sub>2</sub> /UDF (58/29/5/3/5)	561.1 ± 2.1	22.7 ± 0.8	207.5 ± 9.6
PP/rLDPE/MAC/SiO <sub>2</sub> /TTDF (58/29/5/3/5)	644.3 ± 1.0	25.2 ± 1.7	644.3 ± 6.6
PP/rLDPE/MAC/SiO <sub>2</sub> /CTDF (58/29/5/3/5)	613.2 ± 6.8	24.3 ± 1.7	310.5 ± 8.3

were tested (MAC, MAC/SiO<sub>2</sub>, and MAC/SiO<sub>2</sub>/IL). As shown in Table 2, the best results were obtained for the PP/rLDPE (75/25) blend. A significant increase of tensile properties was obtained with the three compatibilizing systems [Young modulus from 503.2 MPa for PP/rLDPE (75/25) to 588.6, 655.4, and 622.0 MPa, respectively, for PP/rLDPE/MAC, PP/rLDPE/MAC/SiO<sub>2</sub>, and PP/rLDPE/MAC/SiO<sub>2</sub>/IL], stress at break (from 25.5 MPa for PP/rLDPE (75/25) to 33.5, 34.1, and 31.8 MPa for, respectively, PP/rLDPE/MAC, PP/rLDPE/MAC/SiO<sub>2</sub>, and PP/rLDPE/MAC/SiO<sub>2</sub>/IL) and elongation at break [from 109.1% for PP/rLDPE (75/25) to 954.6, 883.6, and 844.2 MPa for, respectively, PP/rLDPE/MAC, PP/rLDPE/MAC/SiO<sub>2</sub>, and PP/rLDPE/MAC/SiO<sub>2</sub>/IL]. The presence of MAC, which acted as a dispersing agent between both polymers, thereby improves the interfacial adhesion by which the Young's modulus, stress at break and elongation at break have increased. Zhao et al. [46] studied the effect of various compatibilizers on HDPE, PP, and PVC mixtures and found that the ethylene-glycidyl methacrylate copolymer provides a better interface. The relatively highest improvements of the Young's modulus, stress, and strain at break were observed during the addition of MAC/nano-SiO<sub>2</sub>. MAC acts as a load carrier which further strengthened the composite and also improves the adhesion between the nano-SiO<sub>2</sub> and the polymer favoring a good dispersion of the nano-SiO<sub>2</sub> in the polymer matrix and subsequent restriction in the mobility of the polymer chains [4, 28, 30, 31]. All these features suggest an improvement in the adhesion between the constituents of the polymer blend. With MAC/nano-SiO<sub>2</sub>/ionic liquid, no further improvement of the Young's modulus, stress at break, and elongation at break was observed. On the contrary, a decrease of these three properties was observed compared to the MAC/nano-SiO<sub>2</sub> samples. This is attributed to the presence of IL-TFSI multilayers on the nano-SiO<sub>2</sub> surface that can act as a plasticizer of the interface region between the rigid nano-SiO<sub>2</sub> and the polymer matrix.

In order to investigate the effect of the diss fibers, the PP/rLDPE/MAC/SiO<sub>2</sub> (61.3/30.7/5/3) blend which exhibited the best tensile properties was chosen as the basic blend. The results are given in Table 3. Tensile properties decreased with the addition of diss fibers [Young's modulus from 655.4 MPa for PP/rLDPE/MAC/SiO<sub>2</sub> (61.3/30.7/5/3) to 561.0, 644.3, and 613.2], MPa for, respectively, PP/rLDPE/MAC/SiO<sub>2</sub>/UDF (58/29/5/3/5), PP/rLDPE/MAC/SiO<sub>2</sub>/TTDF (58/29/5/3/5), and PP/rLDPE/MAC/SiO<sub>2</sub>/CTDF (58/29/5/3/5), stress at break [from 34.1 MPa for PP/rLDPE/MAC/SiO<sub>2</sub> (61.3/30.7/5/3) to 22.7, 25.2, and 24.3 MPa for, respectively, PP/rLDPE/MAC/SiO<sub>2</sub>/UDF (58/29/5/3/5), PP/rLDPE/MAC/SiO<sub>2</sub>/TTDF (58/29/5/3/5), and PP/rLDPE/MAC/SiO<sub>2</sub>/CTDF (58/29/5/3/5)], and elongation at break [from 883.6% for PP/rLDPE/MAC/SiO<sub>2</sub> (61.3/30.7/5/3) to 207.5, 644.3, and 310.5% for, respectively, PP/rLDPE/MAC/SiO<sub>2</sub>/UDF (58/29/5/3/5), PP/rLDPE/MAC/SiO<sub>2</sub>/TTDF (58/29/5/3/5), and PP/rLDPE/MAC/SiO<sub>2</sub>/CTD (58/29/5/3/5)]. However, all these properties remained higher than those of the PP/rLDPE blends (50/50 and 75/25). Uniform dispersion of the filler leads to the improvement of the mechanical properties. On the contrary, aggregated filler clusters in the polymer matrix act as concentrator of stress points leading to the deterioration of these properties [60]. On the other hand, the tensile properties obtained in the case of TTDF and CTDF are higher than those obtained with UDF and the properties obtained with TTDF are higher than those obtained with CTDF. It can be seen that the treatment of fibers changed the entire nature of the composites. The treatments caused a decrease of elongation indicating a decrease in the ductility of the composites. The characterization of diss fibers using FTIR spectroscopy showed that the treatments did not modify the fiber surface significantly [47, 54]. Only an increase in crystallinity and removal of moisture occurred for the diss fibers after heat and chemical treatment. An increase in crystallinity of the

**Table 3** Melting temperature ( $T_m$ ), heat of fusion ( $\Delta H_m$ ), crystallization temperature ( $T_c$ ), heat of crystallization ( $\Delta H_c$ ), and degree of crystallinity ( $X_c$ ) of compatibilized PP/rLDPE blends and biocomposites

Formulations	PP phase					rLDPE phase				
	$T_m$ (°C)	$\Delta H_m$ (J/g)	$T_c$ (°C)	$\Delta H_c$ (J/g)	$X$ (%)	$T_m$ (°C)	$\Delta H_m$ (J/g)	$T_c$ (°C)	$\Delta H_c$ (J/g)	$X$ (%)
PP/rLDPE (50/50)	164.6	50.2	123.8	52.1	49.8	130.9	29.8	115.4	24.3	36.2
PP/rLDPE/MAC (47.5/47.5/5)	164.7	28.8	122.8	31.0	29.7	131.4	69.2	115.7	55.9	38.5
PP/rLDPE/MAC/SiO <sub>2</sub> (46/46/5/3)	163.6	32.9	123.9	37.1	35.5	130.3	68.3	117.4	57.8	39.9
PP/rLDPE/MAC/SiO <sub>2</sub> /IL (44.5/44.5/5/3/3)	164.1	29.2	123.6	29.4	28.2	130.7	68.1	116.6	56.0	38.6
PP/r LDPE (75/25)	165.0	34.0	124.8	39.6	25.3	131.8	67.8	116.3	59.2	30.4
PP/r LDPE/MAC (63.3/31.7/5)	164.0	52.0	123.5	54.5	34.7	130.0	28.9	116.8	24.7	34.1
PP/rLDPE/MAC/SiO <sub>2</sub> (61.3/30.7/5/3)	164.0	52.1	123.5	54.2	34.6	129.8	32.5	116.7	26.0	35.8
PP/rLDPE/MAC/SiO <sub>2</sub> /IL (59.3/29.6/5/3/3)	164.6	50.1	122.8	46.4	29.7	130.2	28.0	115.1	18.5	25.5
PP/rLDPE/MAC/SiO <sub>2</sub> /UDF (58/29/5/3/5)	164.7	36.9	122.2	32.2	20.5	131.0	25.9	114.0	15.7	21.7
PP/rLDPE/MAC/SiO <sub>2</sub> /TTDF (58/29/5/3/5)	164.7	45.9	122.5	40.5	25.8	130.1	24.8	115.2	14.1	19.5
PP/rLDPE/MAC/SiO <sub>2</sub> /CTDF (58/29/5/3/5)	164.5	46.0	122.6	40.2	25.6	130.0	24.7	115.0	14.7	20.4

fibers was also observed by Bessadok et al. [52] which causes an improvement in fiber/matrix adhesion of the composites.

### DSC Analysis

Melting and crystallization curves from the second heating and first cooling cycles of the PP/rLDPE blends which were compatibilized using MAC, MAC/SiO<sub>2</sub>, and MAC/SiO<sub>2</sub>/IL and biocomposites were analyzed. The corresponding data are given in Table 3. Interesting characteristics can be obtained from these results. Two melting peaks are apparent in the total heat flow. Both melting ( $T_m$ ) and crystallization temperatures ( $T_c$ ) of PP and rLDPE phases are determined at the maximum of the melting and crystallization peaks from the second heat and cooling DSC thermograms, respectively. Mixtures have endothermic peaks at two different regions. The melting peak at about 132 °C was assigned to the rLDPE and the second peak at about 165 °C to PP in the absence of compatibilizers (MAC, MAC/SiO<sub>2</sub>, and MAC/SiO<sub>2</sub>/IL) in the mixtures. Globally, both  $T_m$  and  $T_c$  of each component in the compatibilized blends and the biocomposites remained practically constant (163.6–164.7 °C and 129.8–131.8 °C, respectively, for  $T_m$  of PP and rLDPE; 122.2–123.8 °C and 114.0–117.4 °C, respectively, for  $T_c$  of PP and rLDPE). These values remained practically constant after the introduction of the compatibilizers, proving their good dispersion in the polymeric matrix. Thus, the melting temperatures stayed in the range of 129.8–131.8 °C and 163.6–164.7 °C for rLDPE and PP, respectively. Likewise, the crystallization temperatures were in the range of 114.0–117.4 °C and 122.2–123.8 °C for the same components. The  $X_c$  of each component in the mixtures lowered when decreasing the content of the corresponding component. A decrease of  $X_c$  of the crystalline components in the mixtures with respect

to the pure polymers is generally observed when there are specific interactions between the components [49].  $X_c$  of each component in the mixture increased with addition of UDF, CTDF, and TTDF, respectively [29]. The heat treatment does not affect the fibers surface very much (Fig. 2). Only an increase in crystallinity and removal of moisture occurred for the diss fibers after heat treatment. The increase in crystallinity for fibers was also observed by Gui et al. [54]. This causes an improvement in fiber/matrix adhesion. The addition of UDF, TTDF, and CTDF to PP/rLDPE affected the crystallinity of the PP and rLDPE.

### TG Characterization

Thermal stability is a very important parameter for polymer materials as it is often the limiting factor for both processing and end-user applications [61]. The corresponding data of the thermograms PP/rLDPE blends compatibilized by MAC, MAC/SiO<sub>2</sub>, and MAC/SiO<sub>2</sub>/IL are given in Table 4. Whatever the compatibilizers introduced in the PP/rLDPE mixture, there was a significant increase in the thermal stability of the polymer materials [491.9, 493.1, and 499.5 °C, respectively, for PP/rLDPE/MAC (63.3/31.7/5), PP/rLDPE/MAC/SiO<sub>2</sub> (61.3/30.7/5/3), and PP/rLDPE/MAC/SiO<sub>2</sub>/IL (59.3/29.7/5/3/3)] compared to PP (360 °C). In fact, the improvement of the thermal stability can be addressed to the barrier effect of SiO<sub>2</sub> [61]. Even MAC acted as a dispersing agent between the polymers resulting in improved interfacial adhesion, and the nano-SiO<sub>2</sub> inhibiting the diffusion of the oxygen molecules necessary to trigger oxidative degradation by creating a “tortuous path” in the matrix [62]. A barrier effect due to nano-SiO<sub>2</sub> may also slow down the rate of mass loss by preventing the escape of the volatile products from the thermal degradation process of the nanocomposites [61]. For MAC/SiO<sub>2</sub>/IL, the temperatures  $T_d$  (347.1 °C), T50%



**Table 4** Thermogravimetric data of compatibilized PP/rLDPE blends and biocomposites

Formulations	$T_d$ (°C)	$T_{10\%}$ (°C)	$T_{50\%}$ (°C)	$T_{max}$ (°C)	$S$ (%/°C)	RR (%)
PP/rLDPE (50/50)	322.5	425.6	464.2	476.2	−0.3	3.2
PP/rLDPE/MAC (47.5/47.5/5)	336.5	446.4	470.6	479.5	−0.2	5.2
PP/rLDPE/MAC/SiO <sub>2</sub> (46/46/5/3)	341.8	452.1	473.6	499.8	−0.3	2.9
PP/rLDPE/MAC/SiO <sub>2</sub> /IL (44.5/44.5/5/3/3)	313.9	429.4	467.4	499.2	−0.2	3.3
PP/rLDPE (75/25)	335.6	429.7	466.3	477.3	0.4	3.1
PP/rLDPE/MAC (63.3/31.7/5)	333.3	444.7	464.4	491.9	−0.3	5.2
PP/rLDPE/MAC/SiO <sub>2</sub> (61.3/30.7/5/3)	354.0	448.7	467.4	493.1	−0.3	2.4
PP/rLDPE/MAC/SiO <sub>2</sub> /IL (59.3/29.6/5/3/3)	347.1	428.2	466.4	499.5	−0.2	3.5
PP/rLDPE/MAC/SiO <sub>2</sub> /UDF(58/29/5/3/5)	332.2	429.4	470.3	498.7	−0.3	6.5
PP/rLDPE/MAC/SiO <sub>2</sub> /TTDF(58/29/5/3/5)	354.6	436.7	470.3	499.8	−0.3	6.4
PP/rLDPE/MAC/SiO <sub>2</sub> /CTDF(58/29/5/3/5)	350.2	427.7	465.7	495.9	−0.3	4.2

$T_d$  degradation onset temperature,  $T_{10\%}$  temperature at 10% mass loss,  $T_{50\%}$  temperature at 50% mass loss,  $T_{max}$  maximum decomposition temperature,  $S$  degradation speed,  $RR$  residual rate

(466.6 °C), and  $T_{max}$  (499.6 °C) are improved. This is probably attributed to a better dispersion of nano-SiO<sub>2</sub> which increases the length of the tortuous path that prevents the diffusion of decomposition gases [63]. Another reason for this improvement could be the greater thermal stability of IL-TFSI [64]. These phosphonium ionic liquids with long alkyl chains (scheme 1) are used here as novel compatibilizing agents in polymer blends. By controlling the chemical nature of the counter anion, the intrinsic thermal stability of the ionic liquids was studied. According to the literature, the combination of the anion associated with the organic cation plays a fundamental role on the thermal stability of the phosphonium salts [66–68]. In fact, the use of the TFSI anion combined with the phosphonium cation results in an increase of the degradation temperature of about 20 °C, over the compatibilized mixtures by MAC which is decreased to about 479.6 °C. Many Authors reported similar results [65]. The use of ionic liquids associated with fluorinated anions such as hexafluoro phosphate (PF 6) or tetra fluoro borate (BF<sub>4</sub>) was reported [42, 68]. Recently, Livi et al. [42] pointed out that the replacement of the halide anion (Br, I) by a fluorinated phosphonium anion increases the thermal stability of its composites. Table 4 shows that the onset temperature of PP/rLDPE/MAC/SiO<sub>2</sub> (61.3/30.7/5/3) blend is about 354.3 °C, and the DTG curve in Table 4 shows a two-step degradation at around 368.0 °C for rLDPE and 474.0 °C for PP. The composite reinforced with 5% diss fibers shows a decrease of onset degradation but increase of maximal temperature of PP. This result indicates that the stability of the composites is affected by the addition of small amounts of diss fibers. On the other hand, the temperature at 10% mass loss of the biocomposite PP/rLDPE/MAC/SiO<sub>2</sub>/TTDF (58/29/5/3/5) (436.7 °C) is higher than the temperature at 10% mass loss of both biocomposites PP/rLDPE/MAC/SiO<sub>2</sub>/UDF (58/29/5/3/5) (429.4 °C) and PP/rLDPE/MAC/SiO<sub>2</sub>/

CTDF (58/29/5/3/5) (427.7 °C) which suggests that the thermal stability is better in presence of the TTDF.

### XRD Characterization

X-ray diffraction is used for characterizing the structural changes occurring in crystalline polymers as a result of mixing. The X-ray diffraction pattern of PP/rLDPE mixtures compatibilized by MAC, MAC/SiO<sub>2</sub>, and MAC/nano-SiO<sub>2</sub>/IL is illustrated in Fig. 4 by a Bragg angle function ( $2\theta$ ) and the corresponding data were shown in Table 5. For rLDPE, two typical peaks at  $2\theta = 21.4^\circ$  and  $23.6^\circ$  corresponding respectively to the crystallographic planes (110) and (200) of the orthorhombic form of polyethylene superimposed on the amorphous halo are observed [69]. The diffraction

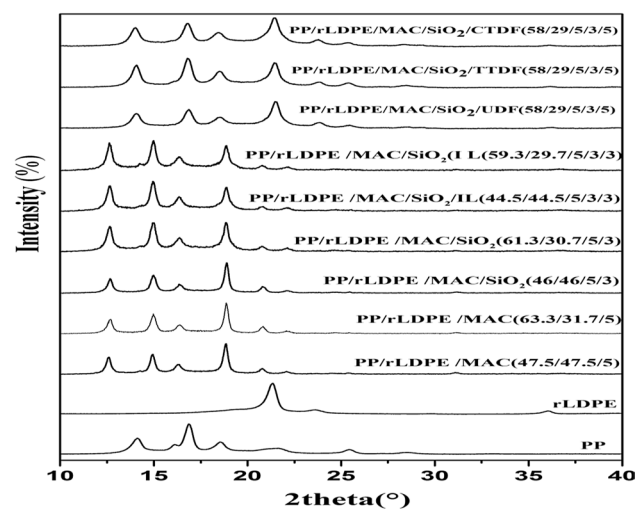


**Fig. 4** X-ray diffraction of compatibilized PP/rLDPE-based blends and biocomposites

**Table 5** Crystallinity ( $X_c$  %) of compatibilized PP/rLDPE blends and biocomposites

Formulations	PP ( $X_c$ %) crystallinity	rLDPE ( $X_c$ %) crystallinity
PP	38.6	–
rLDPE	–	53.4
PP/rLDPE/MAC (47.5/47.5/5)	29.5	38.3
PP/rLDPE/MAC/SiO <sub>2</sub> (46/46/5/3)	35.3	39.7
PP/rLDPE/MAC/SiO <sub>2</sub> /IL (44.5/44.5/5/3/3)	28.0	38.4
PP/r LDPE/MAC (63.3/31.7/5)	34.5	34.4
PP/rLDPE/MAC/SiO <sub>2</sub> (61.3/30.7/5/3)	34.5	35.5
PP/rLDPE/MAC/SiO <sub>2</sub> /IL (59.3/29.6/5/3/3)	29.4	25.3
PP/rLDPE/MAC/SiO <sub>2</sub> /UDF (58/29/5/3/5)	20.3	21.9
PP/rLDPE/MAC/SiO <sub>2</sub> /TTDF (58/29/5/3/5)	25.7	19.3
PP/rLDPE/MAC/SiO <sub>2</sub> /CTDF (58/29/5/3/5)	25.3	20.2

peaks at  $2\theta = 14.2^\circ$ ,  $17.0^\circ$ ,  $18.8^\circ$ , and  $20.0^\circ$  were assigned respectively to the (110), (040), (130), and (111) planes of a PP crystal. The peaks of recovery between  $21.1^\circ$  and  $22.1^\circ$  were correlated to a combination of phase  $\alpha$  (131 and 041) and phase  $\beta$  (301) of PP. Finally the small peak observed at  $25.4^\circ$  was related to the  $\alpha$  form of PP (060) [70]. By adding the compatibilizers (Fig. 4), the curve remains the same as before. Consequently, compatibilizers could not alter the crystal structure of this binary mixture. Concerning nano-SiO<sub>2</sub>, a single reflection peak at  $2\theta = 26.5^\circ$  can be observed for the mixtures. Thus, the absence of the ‘intercalated’ diffraction peak at a value less than  $2\theta$  suggests that the nano-SiO<sub>2</sub> is expanded to the processing temperature during melt blending. Moreover, no new diffraction peaks could be observed for PP/rLDPE mixtures indicating that the use of nano-SiO<sub>2</sub> fillers has no significant influence on the crystal structure of PP/rLDPE blends. However, variations in the relative intensity of the diffraction peaks of the PP/rLDPE matrix caused by the addition of MAC, nano-SiO<sub>2</sub> and IL may affect the degree of crystallinity and therefore may affect the final physical properties of the resulting composites. The addition of fibers (UDF, TTDF, and CTDF) does not affect the shape of the curve as shown in Fig. 4. Consequently, UDF, CTDF, and TTDF could not alter the crystal structure of this binary mixture. For nano-SiO<sub>2</sub>, a single reflection peak at  $2\theta = 26.5^\circ$  can be observed for the mixtures, so that the absence of the diffraction peak at a value less than  $2\theta$  suggests that the nano-SiO<sub>2</sub> is dispersed as the temperature increases during melt blending. Moreover, no new diffraction peaks can be observed for PP/rLDPE mixtures indicating that the use of nano-SiO<sub>2</sub> fillers has no

appreciable influence on the crystal structure of PP/rLDPE. However, variations in the relative intensity of the diffraction peaks of the PP/rLDPE matrix caused by the addition of UDF, TTDF, and CTDF may affect the degree of crystallinity and therefore may affect the final physical properties of the resulting composites.

### SEM Analysis

The morphology of the compatibilized mixtures was observed by SEM in order to evaluate the dispersion state of MAC, nano-SiO<sub>2</sub>, and IL-TFSI in the PP/rLDPE matrix as well as the evolution of dispersion and interfacial adhesion between PP and rLDPE. The problem of agglomeration of the hydrophilic nano-SiO<sub>2</sub> in the polymer matrix seems to be due to their differences with the polymers and their high surface-to-volume ratio. For example, physical mixing of the hydrophobic polymers (PP and rLDPE) with nano-SiO<sub>2</sub> hydrophilic inorganic particles can lead to nano-fillers-phase separation or agglomeration of particles which result in poor mechanical properties. In addition, high surface energy particles are easily agglomerated as the amount of particles increases due to the nanoscopic size of the charges leading to a large specific surface area followed by a further increase in interfacial tension. This results in higher filler–filler interactions assigned to hydrogen bonds and Van Der Waals interactions, but conversely, in poor interactions between the hydrophobic polymer chains and the hydrophilic nano-SiO<sub>2</sub>. The addition of MAC leads to a relatively uniform dispersion (Fig. 5a). The average size of the nano-SiO<sub>2</sub> agglomerates was decreased and a homogeneous dispersion of moderately sized aggregates of nano-fillers appeared. In addition, the nano-SiO<sub>2</sub> appears to be well emerged in the PP/rLDPE with uniform size. It can be noted that the nano-fillers are still aggregated even with use of a compatibilizing copolymer. However, it is clear that the size of the nano-SiO<sub>2</sub> population is reduced and that the nanoparticles form small aggregates. These results suggest that the MAC coupling agent is very useful and has a significant effect on the dispersion process. With the help of MAC, reduction of interfacial tension and improvement of interfacial adhesion are simultaneously observed. In fact, this copolymer must be located in the interfacial zone between PP/rLDPE and nano-SiO<sub>2</sub> due to polar interactions such as hydrogen bonds occurring between the carboxyl groups of the grafting agent and the surface hydroxyl groups of nano-SiO<sub>2</sub>, as well as the interactions between the polypropylene chains and the non-polar parts of the grafting agent. The improvement of the dispersion state and the homogenization of the particle size distribution of the nano-SiO<sub>2</sub> aggregates using a grafting agent observed in this study are similar to those reported by Byrne and McNally [67] in their study on the effect of maleic polypropylene on the mechanical and morphological

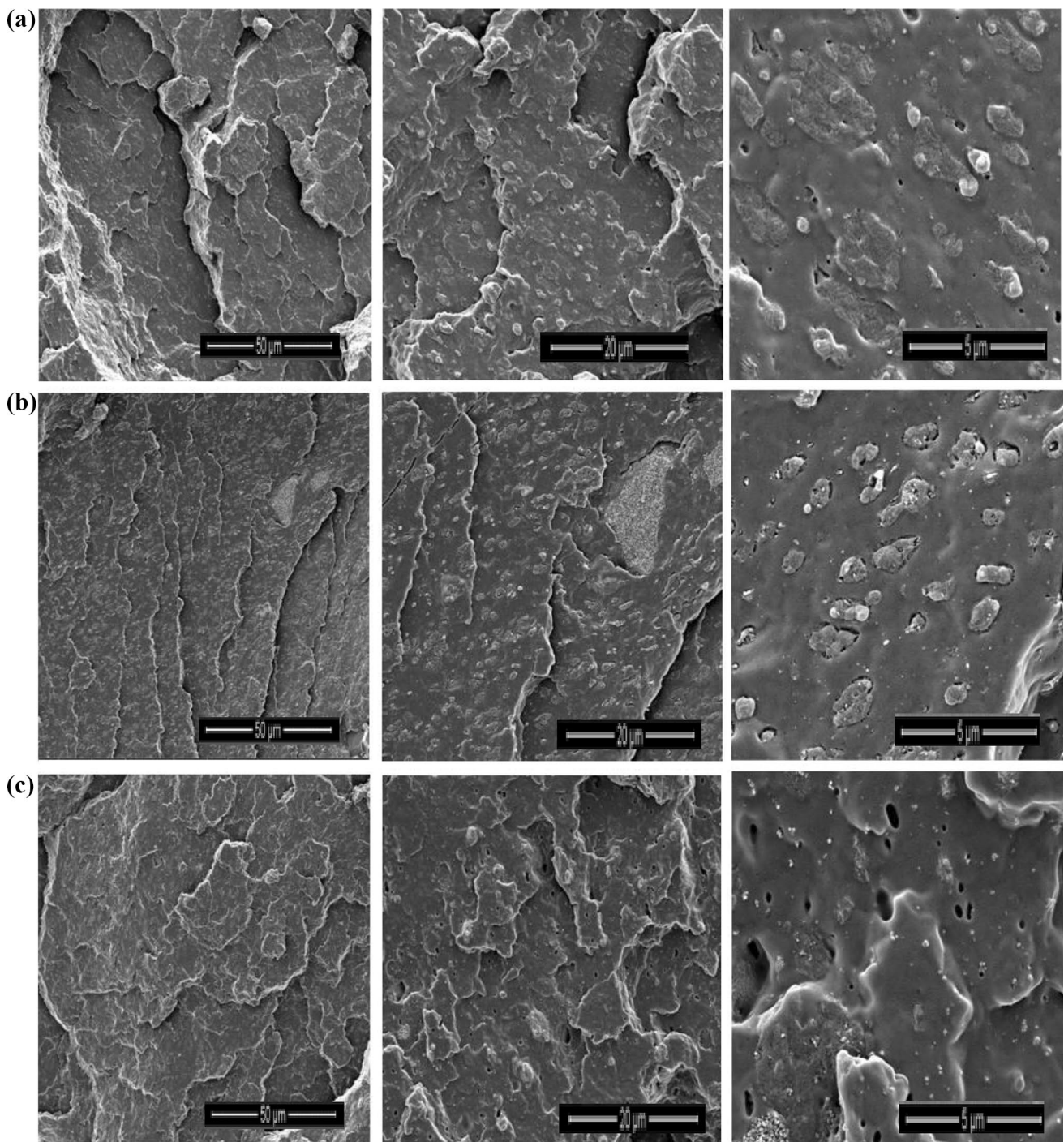
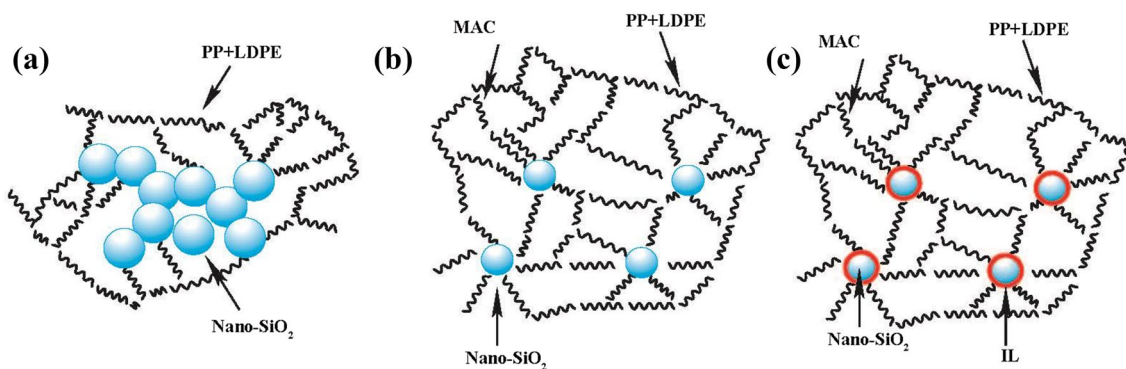


**Fig. 5** SEM micrographs of compatibilized blends: **a** PP/rLDPE/MAC (63.3/31.7/5), **b** PP/r LDPE/MAC/SiO<sub>2</sub> (61.3/30.7/5/3), and **c** PP/r LDPE/MAC/SiO<sub>2</sub>/IL (59.3/29.7/5/3/3)

properties of PA6/PP/organo-granulated injection-molded nanocomposites. More recently, Leroy et al. [29] showed that the use of nanoparticles in a mixture of polymers acts as an emulsifier that stabilizes the mixture [29].

Finally, ionic liquids act as compatibilizers because their accumulation at the interphase contributes to the

formation of a barrier around the minor phase which hinders the coalescence of the rLDPE domains leading to the formation of smaller particles (Fig. 5b, c and Scheme 3). In addition, a small amount of ionic liquid is required to improve the compatibilization of PP/rLDPE blends [60–62].



**Scheme 3** Schematic representation of the effect of **a** MAC, **b** MAC/SiO<sub>2</sub> and **c** MAC/SiO<sub>2</sub>/ionic liquid on PP/rLDPE blends

## Conclusion

Based on the disposal of waste plastic and valorization of diss fibers, blending the recycled and regenerated low-density polyethylene rLDPE and PP by a twin-screw extruder with different compatibilizers was succeeded. Among the tested compatibilizers (MAC, MAC/SiO<sub>2</sub>, and MAC/SiO<sub>2</sub>/IL), the best results for the PP/rLDPE (75/25) blend were obtained with MAC/SiO<sub>2</sub> (5/3) which seems to strengthen the interactions between rLDPE and PP. The tensile strength, Young's modulus, and interfacial bonding between PP and rLDPE were the best. The stability of the composites was affected by the incorporation of 5% diss fibers. It seems that diss fibers exert a stabilizing effect on the thermal degradation of the biocomposites. Finally, the PP/rLDPE composites reinforced with diss fibers exhibited good mechanical properties and satisfactory adhesion. Then, from the point of view of practical applications, the use of diss fibers in developing PP/rLDPE biobased composites is an effective way of valorization of diss fibers and regenerated LDPE.

**Funding** The funding was provided by Direction Générale de la Recherche Scientifique et du Développement Technologique.

## References

- Zhao, J., Chen, M., Wang, X., Zhao, X., Wang, Z., Dang, Z.-M., Ma, L., Hu, G.-H., Chen, F.: Triple shape memory effects of cross-linked polyethylene/polypropylene blends with cocontinuous architecture. *ACS Appl. Mater. Interfaces* **5**, 5550–5556 (2013)
- Thakur, V.K., Vennerberg, D., Kessler, M.R.: Green aqueous surface modification of polypropylene for novel polymer nanocomposites. *ACS Appl. Mater. Interfaces* **6**, 9349–9356 (2014)
- Himma, N.F., Anisah, S., Prasetya, N., Wenten, I.G.: Advances in preparation, modification, and application of polypropylene membrane. *J. Polym. Eng.* **36**, 329–362 (2015)
- Pedrazzoli, D., Pegoretti, A.: Silica nanoparticles as coupling agents for polypropylene/glass composites. *Compos. Sci. Technol.* **76**, 77–83 (2013). <https://doi.org/10.1016/j.compscitech.2012.12.016>
- Izzati Zulkifli, N., Samat, N., Anuar, H., Zainuddin, N.: Mechanical properties and failure modes of recycled polypropylene/microcrystalline cellulose composites. *Mater. Des.* **69**, 114–123 (2015). <https://doi.org/10.1016/j.matdes.2014.12.053>
- Maani, A., Naguib, H.E., Heuzey, M.C., Carreau, P.J.: Foaming behavior of microcellular thermoplastic olefin blends. *J. Cell. Plast.* **49**, 223–244 (2013). <https://doi.org/10.1177/0021955X13477435>
- Blom, H.P., Teh, J.W., Rudin, A., PP/PE blends. IV. Characterization and compatibilization of blends of postconsumer resin with virgin PP and HDPE. *J. Appl. Polym. Sci.* **70**, 2081–2095 (1998)
- Al-Salem, S.M., Lettieri, P., Baeyens, J.: Recycling and recovery routes of plastic solid waste (PSW): a review. *Waste Manag.* **29**, 2625–2643 (2009). <https://doi.org/10.1016/j.wasman.2009.06.004>
- Mustafa, N.: Plastic Waste Management. Canadian Plastics Institute, Toronto (1993)
- John, S.: Polymer Recycling. Wiley, Chichester (1998)
- Yu, M., Huang, R., He, C., Wu, Q., Zhao, X.: Hybrid composites from wheat straw, inorganic filler, and recycled polypropylene: morphology and mechanical and thermal expansion performance. *Int. J. Polym. Sci.* (2016). <https://doi.org/10.1155/2016/2520670>
- Xu, B., Lin, Z., Xian, J., Huo, Z., Cao, L., Wang, Y., Gaosun, W., Mai, K., Wang, Y.: Preparation and characterization of polypropylene composites with nonmetallic materials recycled from printed circuit boards. *J. Thermoplast. Compos. Mater.* **29**, 48–57 (2016). <https://doi.org/10.1177/0892705713518788>
- Salmah, H., Azra, B.N., Yusrina, M.D., Ismail, H.: A comparative study of polypropylene/(chloroprene rubber) and (recycled polypropylene)/(chloroprene rubber) blends. *J. Vinyl Addit. Technol.* **21**, 122–127 (2015). <https://doi.org/10.1002/vnl.21390>
- Garlof, S., Mecklenburg, M., Smazna, D., Mishra, Y.K., Adelung, R., Schulte, K., Fiedler, B.: 3D carbon networks and their polymer composites: fabrication and electromechanical investigations of neat Aerographite and Aerographite-based PNCs under compressive load. *Carbon* **111**, 103–112 (2017)
- Thakur, V.K., Singha, A.S., Thakur, M.K.: In-air graft copolymerization of ethyl acrylate onto natural cellulosic polymers. *Int. J. Polym. Anal. Charact.* **17**, 48–60 (2012)
- Parlak, O., Kumar Mishra, Y., Grigoriev, A., Mecklenburg, M., Luo, W., Keene, S., Salleo, A., Schulte, K., Ahuja, R., Adelung, R., Turner, A.P.F., Tiwari, A.: Hierarchical Aerographite nanomicrotubular tetrapodal networks based electrodes as lightweight supercapacitor. *Nano Energy* **34**, 570–577 (2017)

17. Thakur, V.K., Singha, A.S., Thakur, M.K.: Surface modification of natural polymers to impart low water absorbency. *Int. J. Polym. Anal. Charact.* **17**, 133–143 (2012)
18. Singha, A.S., Thakur, V.K.: Mechanical, thermal and morphological properties of grevia optiva fiber/polymer matrix composites. *Polym. Plast. Technol. Eng.* **48**, 201–208 (2009). <https://doi.org/10.1080/03602550802634550>
19. Sellami, A., Merzoud, M., Amziane, S.: Improvement of mechanical properties of green concrete by treatment of the vegetal fibers. *Constr. Build. Mater.* **47**, 1117–1124 (2013). <https://doi.org/10.1016/j.conbuildmat.2013.05.073>
20. Bertin, S., Robin, J.J.: Study and characterization of virgin and recycled LDPE/PP blends. *Eur. Polym. J.* **38**, 2255–2264 (2002)
21. Shanks, R.A., Li, J., Chen, F., Amarasinghe, G.: Time-temperature-miscibility and morphology of polyolefin blends. *Chin. J. Polym. Sci.* **18**, 263–270 (2000)
22. Guerfi, N., Belhaneche-Bensemra, N.: Preparation, characterization and valorization of regenerated low density polyethylene/polypropylene blends. *Environ. Eng. Manag. J.* **13**, 2609–2613 (2014)
23. Radonjic, G., Gubeljak, N.: The use of ethylene/propylene copolymers as compatibilizers for recycled polyolefin blends. *Macromol. Mater. Eng.* **287**, 122–132 (2002)
24. Vaccaro, E., Dibenedetto, A.T., Huang, S.J.: Yield strength of low-density polyethylene-polypropylene blends. *J. Appl. Polym. Sci.* **63**, 275–281 (1997)
25. Yang, M.B., Wang, K., Ye, L., Mai, Y.W., Wu, J.S.: Low density polyethylene-polypropylene blends part 2—strengthening and toughening with copolymer. *Plast. Rubber Compos.* **32**, 27–31 (2003)
26. Elias, L., Fenouillot, F., Majeste, J.C., Cassagnau, P.: Morphology and rheology of immiscible polymer blends filled with silica nanoparticles. *Polymer* **48**, 6029–6040 (2007)
27. Yang, H., Zhang, X., Qu, C., Li, B., Zhang, L., Zhang, Q.: Largely improved toughness of PP/EPDM blends by adding nano-SiO<sub>2</sub> particles. *Polymer* **48**, 860–869 (2007)
28. Jose, S., Thomas, S., Biju, P.K., Karger-Kocsis, J.: Mechanical and dynamic mechanical properties of polyolefin blends: effect of blend ratio and copolymer monomer fraction on the compatibilisation efficiency of random copolymers. *J. Polym. Res.* **20**, 303 (2013). <https://doi.org/10.1007/s10965-013-0303-5>
29. Safadi, B., Andrews, R., Grulke, E.A.: Multiwalled carbon nanotube polymer composites: synthesis and characterization of thin films. *J. Appl. Polym. Sci.* (2002). <https://doi.org/10.1002/app.10436>
30. Thankappan Nair, S., Vijayan, P.P., Xavier, P., Bose, S., George, S.C., Thomas, S.: Selective localisation of multi walled carbon nanotubes in polypropylene/natural rubber blends to reduce the percolation threshold. *Compos. Sci. Technol.* **116**, 9–17 (2015). <https://doi.org/10.1016/j.compscitech.2015.04.021>
31. Dorigato, A., Pegoretti, A., Frache, A.: Thermal stability of high density polyethylene-fumed silica nanocomposites. *J. Therm. Anal. Calorim.* **109**, 863–873 (2012). <https://doi.org/10.1007/s10973-012-2421-4>
32. Dorigato, A., Pegoretti, A.: Reprocessing effects on propylene/silica nanocomposites. *J. Appl. Polym. Sci.* (2014). <https://doi.org/10.1002/APP.40242>
33. Jeziórska, R., Świerż-Motysia, B., Zielecka, M., Szadkowska, A., Studziński, M.: Structure and mechanical properties of low-density polyethylene/spherical silica nanocomposites prepared by melt mixing: the joint action of silica's size, functionality, and compatibilizer. *J. Appl. Polym. Sci.* **125**, 4326–4337 (2012). <https://doi.org/10.1002/app.36579>
34. Daramola, O.O., Oladele, I.O., Adewuyi, B.O., Sadiku, R., Agwuncha, S.C.: Thermal, structural and morphological properties of high density polyethylene matrix composites reinforced with submicron agro silica particles and Titania particles. *J. Taihah Univ. Sci.* **11**, 645–653 (2017). <https://doi.org/10.1016/j.jtusc.i.2016.08.006>
35. Vladimirov, V., Betchev, C., Vassiliou, A., Papageorgiou, G., Bikiaris, D.: Dynamic mechanical and morphological studies of isotactic polypropylene/fumed silica nanocomposites with enhanced gas barrier properties. *Compos. Sci. Technol.* **66**, 2935–2944 (2006). <https://doi.org/10.1016/j.compscitech.2006.02.010>
36. Kurokawa, Y., Yasuda, H., Oya, A.J.: Preparation of a nanocomposite of polypropylene and smectite. *J. Mater. Sci. Lett.* **15**, 1481–1483 (1996)
37. Ray, S.S., Okamoto, M.: Polymer/layered silicate nanocomposites: a review from preparation., *Prog. Polym. Sci.* (2003). <https://doi.org/10.1016/j.progpolymsci.2003.08.002>
38. Jain, S., Goossens, H., Picchioni, F., Magusin, P., Mezari, B., Van Duin, M.: Synthetic aspects and characterization of polypropylene-silica nanocomposites prepared via solid-state modification and sol-gel reactions. *Polymer* **46**, 6666 (2005)
39. Jankong, S., Srikulkit, K.: Preparation of polypropylene/hydrophobic silica nanocomposites. *J. Met. Mater. Miner.* **18**, 143–146 (2008)
40. Kato, M., Usuki, A., Okada, A.: Synthesis of polypropylene oligomer—clay intercalation compounds. *J. Appl. Polym. Sci.* **66**, 1781–1785 (1997)
41. Livi, S., Duchet-Rumeau, J., Pham, T.N., Gerard, J.F.: A comparative study on different ionic liquids used as surfactants: effect on thermal and mechanical properties of high-density polyethylene nanocomposites. *J. Colloid Interface Sci.* **349**, 424–433 (2010)
42. Livi, S., Gerard, J.F., Duchet-Rumeau, J.: Ionic liquids: structuration agents in a fluorinated matrix. *Chem. Commun.* **47**, 3589–3591 (2011)
43. Livi, S., Duchet-Rumeau, J., Pham, T.N., Gerard, J.F.: Synthesis and physical properties of new surfactants based on ionic liquids: improvement of thermal stability and mechanical behaviour of high density polyethylene nanocomposites., *J. Colloid Interface Sci.* (2011) <https://doi.org/10.1016/j.jcis.2010.10.058>
44. Rahman, M., Brazel, C.S.: Ionic liquids: new generation stable plasticizers for poly (vinyl chloride). *Polym. Degrad. Stab.* **91**, 3371–3382 (2006)
45. Yao, M., Fan, M., Liang, Y., Zhou, F., Xia, Y.: Imidazolium hexafluorophosphat ionic liquids as high temperature lubricants for steel-steel contacts. *Wear* **268**, 67–71 (2010)
46. Xing, C., Zhao, L., You, J., Dong, W., Cao, X., Li, Y.: Impact of ionic liquid-modified multiwalled carbon nanotubes on the crystallization behavior of poly(vinylidene fluoride). *J. Phys. Chem. B* **116**, 8312–8320 (2012)
47. Xing, C., Zhao, M., Zhao, L., You, J., Cao, X., Li, Y.: Ionic liquid modified poly(vinylidene fluoride): crystalline structures, miscibility, and physical properties. *Polym. Chem.* **4**, 5726–5734 (2013)
48. Zhao, L., Li, Y., Cao, X., You, J., Dong, W.: Multifunctional role of an ionic liquid in melt-blended poly (methyl methacrylate)/ multi-walled carbon nanotube nanocomposites. *Nanotechnology* (2012). <https://doi.org/10.1088/0957-4484/23/25/255702>
49. Leroy, E., Jacquet, P., Coativy, G., Reguerre, A.L., Lourdin, D.: Compatibilization of starch-zein melt processed blends by an ionic liquid used as plasticizer. *Carbohydr. Polym.* **89**, 955–963 (2012)
50. Marinelli, A.L., Bretas, R.E.S.: Blends of polypropylene resins with a liquid crystalline polymer. I. Isothermal crystallization., *J. Appl. Polym. Sci.* (2003). <https://doi.org/10.1002/app.11386>
51. Hung, K.-C., Wu, T.-L., Chen, Y.-L., Wu, J.-H.: Assessing the effect of wood acetylation on mechanical properties and extended creep behavior of wood/recycled-polypropylene composites. *Constr. Build. Mater.* **108**, 139–145 (2016)
52. Bessadok, A., Marais, S., Roudesli, S., Lixon, C., Métayer, M.: Influence of chemical modifications on water-sorption and

- mechanical properties of Agave fibres. *Compos. A* **39**, 29–45 (2008)
53. Hejun, W., Mei, L., Canhui, L.: Non-isothermal crystallization kinetics of peroxide-crosslinked polyethylene: effect of solid state mechanochemical milling. *Thermochim. Acta* (2012). <https://doi.org/10.1016/j.tca.2012.07.008>
  54. Zhao, J., Chen, M., Wang, X., Zhao, X., Wang, Z., Dang, Z.M., Ma, L., Hu, G.H., Chen, F.: Triple shape memory effects of cross-linked polyethylene/polypropylene blends with cocontinuous architecture. *ACS Appl. Mater. Interfaces* (2013). <https://doi.org/10.1021/am400769j>
  55. Gui, Z., Wang, H., Gao, Y., et al.: Morphology and melt rheology of biodegradable poly(lactic acid)/poly(butylenes succinate adipate) blends: effect of blend composition. *Iran. Polym. J.* **21**, 81–89 (2012)
  56. Olsson, A.M., Salmén, L.: The association of water to cellulose and hemicellulose in paper examined by FTIR spectroscopy. *Carbohydr. Res.* (2004). <https://doi.org/10.1016/j.carres.2004.01.005>
  57. Garside, P., Wyeth, P.: Identification of cellulosic fibres by FTIR spectroscopy: thread and single fibre analysis by attenuated total reflectance. *Stud. Conserv.* **48**(4), 269–275 (2003)
  58. Garside, P., Wyeth, P.: Identification of cellulosic fibres by FTIR spectroscopy: thread and single fibre analysis by attenuated total reflectance. *Stud. Conserv.* **48**, 269–275 (2006)
  59. Bessadok, A., Marais, S., Gouanve, F., Colasse, L., Zimmerlin, I., Roudesli, S., et al.: Effect of chemical treatments of Alfa (*Stipa tenacissima*) fibres on water-sorption properties. *Compos. Sci. Technol.* (2006). <https://doi.org/10.1016/j.compscitech.2006.04.013>
  60. Sreekumar, P.A., Saiiah, R., Saiter, J.M., Leblanc, N., Joseph, K., Unnikrishnan, G., et al.: Thermal behaviour of treated and untreated sisal fiber reinforced polyester composites fabricated by resin transfer moulding. *Compos. Interfaces* **15**, 629–650 (2008)
  61. Shi, X., Gan, Z.: Preparation and characterization of poly (propylene carbonate)/montmorillonite nanocomposites by solution intercalation. *Eur. Polym. J.* **43**, 4852–4858 (2007)
  62. Reza Dadfar, S.M., Ahmad Ramazani, S.A., Ali Dadfar, S.M.: Investigation of oxygen barrier properties of organoclay/HDPE/EVA nanocomposite films prepared using a two-step solution method. *Polym. Compos.* (2008). <https://doi.org/10.1002/pc.20711>
  63. Santos, K., Bischoff, E., Liberman, S., Oviedo, M., Mauler, R.: The effects of ultrasound on organoclay dispersion in the PP matrix. *Ultrason. Sonochem.* **18**, 997–1001 (2011)
  64. Kim, N.H., Malhotra, S.V., Xanthos, M.: Modification of cationic nanoclays with ionic liquids. *Microporous Mesoporous Mater.* **96**, 29–35 (2006)
  65. Awad, W.H., Gilman, J.W., Nyden, M., Harris, R.H., Sutto, T.E., Callahan, J., Trulove, P.C., DeLong, H.C., Fox, D.M.: Thermal degradation studies of alkylimidazolium salts and their application in nanocomposites. *Thermochim. Acta* **409**, 3–11 (2004)
  66. Awad, W.H., Gilman, J.W., Nyden, M., Davis, R., Harris, R.H., Sutto, T.E., Callahan, J.H., Delong, H.C., Trulove, P.C.: Thermal degradation studies of alkyl imidazolium salts and their application in nanocomposites. *Molten Salts* **13**, 200–212 (2002)
  67. Xie, W., Xie, R.C., Pan, W.P., Hunter, D., Koene, B., Tan, L.S., Vaia, R.: Thermal stability of quaternary phosphonium modified montmorillonites. *Chem. Mater.* **14**, 4837–4845 (2002)
  68. Byrne, C., McNally, T.: Ionic liquid modification of layered silicates for enhanced thermal stability. *Macromol. Rapid Commun.* **28**, 780–784 (2007)
  69. Rizzo, P., Baione, F., Guerra, G., Martinotto, L., Albizzati, E.: Polyethylene unit cell and crystallinity variations as a consequence of different cross-linking processes. *Macromolecules* **34**, 5175–5179 (2001)
  70. Song, P., Cao, Z., Cai, Y., Zhao, L., Fang, Z., Fu, S.: Fabrication of exfoliated grapheme based polypropylene nanocomposites with enhanced mechanical and thermal properties. *Polymer* (2011). <https://doi.org/10.1016/j.polymer.2011.06.045>